Isolating the effects of reactivity stratification in reactivity-controlled compression ignition with iso-octane and n -heptane on a light-duty multi-cylinder engine

Martin Wissink, Scott Curran, Greg Roberts, Mark Pb Musculus, Christine Mounaïm-Rousselle

International Journal of ENGINE RESEARCH

Standard Article

International J of Engine Research
2018, Vol. 19(9) 907–926

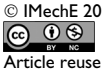

DOI: 10.1177/1468087417732898
journals.sagepub.com/home/jer
SAGE

Isolating the effects of reactivity stratification in reactivity-controlled compression ignition with iso-octane and *n*-heptane on a light-duty multi-cylinder engine*

Martin L Wissink[1], Scott J Curran[1], Greg Roberts[2], Mark PB Musculus[2] and Christine Mounaïm-Rousselle[3]

Abstract

Reactivity-controlled compression ignition (RCCI) is a dual-fuel variant of low-temperature combustion that uses in-cylinder fuel stratification to control the rate of reactions occurring during combustion. Using fuels of varying reactivity (autoignition propensity), gradients of reactivity can be established within the charge, allowing for control over combustion phasing and duration for high efficiency while achieving low NO_x and soot emissions. In practice, this is typically accomplished by premixing a low-reactivity fuel, such as gasoline, with early port or direct injection, and by direct injecting a high-reactivity fuel, such as diesel, at an intermediate timing before top dead center. Both the relative quantity and the timing of the injection(s) of high-reactivity fuel can be used to tailor the combustion process and thereby the efficiency and emissions under RCCI. While many combinations of high- and low-reactivity fuels have been successfully demonstrated to enable RCCI, there is a lack of fundamental understanding of what properties, chemical or physical, are most important or desirable for extending operation to both lower and higher loads and reducing emissions of unreacted fuel and CO. This is partly due to the fact that important variables such as temperature, equivalence ratio, and reactivity change simultaneously in both a local and a global sense with changes in the injection of the high-reactivity fuel. This study uses primary reference fuels iso-octane and *n*-heptane, which have similar physical properties but much different autoignition properties, to create both external and in-cylinder fuel blends that allow for the effects of reactivity stratification to be isolated and quantified. This study is part of a collaborative effort with researchers at Sandia National Laboratories who are investigating the same fuels and conditions of interest in an optical engine. This collaboration aims to improve our fundamental understanding of what fuel properties are required to further develop advanced combustion modes.

Keywords

Reactivity-controlled compression ignition, low-temperature combustion, advanced compression ignition, primary reference fuel, stratification, multi-cylinder

Date received: 26 May 2017; accepted: 18 July 2017

Introduction

Low-temperature combustion (LTC) modes have shown promise in reducing engine out NO_x and soot emissions relative to conventional diesel combustion while demonstrating high brake thermal efficiency (BTE). Despite these advantages, there remain challenges with LTC development, including control authority over combustion phasing, duration, and stability; limited speed/load range; high combustion noise; and high unburned hydrocarbons (HC) and CO emissions. There are a variety of approaches to achieving LTC, and they address these challenges in different

[1]Fuels, Engines, and Emissions Research Center, Oak Ridge National Laboratory, Knoxville, TN, USA
[2]Combustion Research Facility, Sandia National Laboratories, Livermore, CA, USA
[3]Laboratoire PRISME, Université d'Orléans, Orléans, France

Corresponding author:
Martin L Wissink, Fuels, Engines, and Emissions Research Center, Oak Ridge National Laboratory, 2360 Cherahala Blvd, Knoxville, TN 37830, USA.
Email: wissinkml@ornl.gov

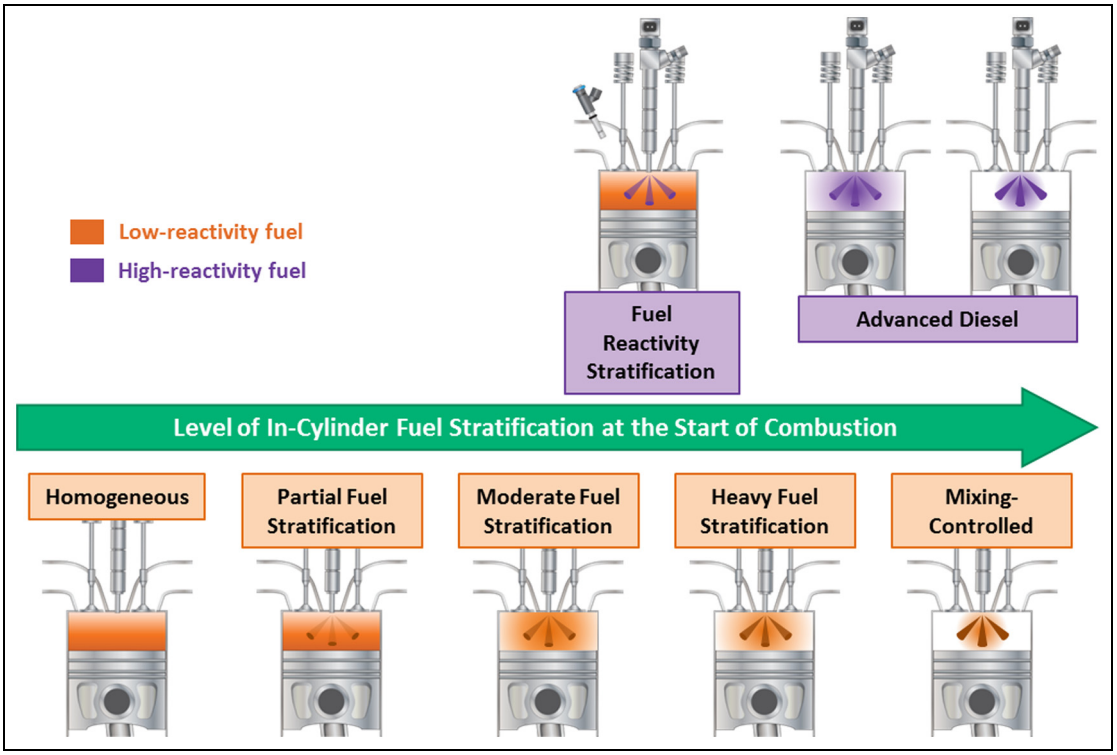

Figure 1. Landscape of advanced compression ignition combustion strategies aimed at achieving low-temperature combustion with gasoline and diesel fuel.
Source: Adapted from Dempsey et al.[1]

ways.[1] Fuel properties best suited to each approach can depend on the performance criteria. With single-fuel strategies, controlling the level of in-cylinder equivalence ratio and temperature stratification through direct injection (DI) timing can allow the combustion mode to traverse a spectrum from kinetically-controlled homogeneous charge compression ignition (HCCI) to mixing-limited combustion, as shown in Figure 1. Dual-fuel approaches provide additional control authority by allowing a gradient of fuel composition to be used in addition to equivalence ratio and temperature stratification. One such strategy, reactivity-controlled compression ignition (RCCI) is most commonly characterized by a premixed charge of a low-reactivity fuel (resistant to autoignition) and the DI of a high-reactivity fuel (promotes autoignition).[2] This approach, which offers the ability to change the global fuel composition via the ratio of the two fuels and to change the stratification of equivalence ratio via the timing of the DI fuel, has been shown to provide additional control over combustion phasing and duration relative to single-fuel strategies. With RCCI, there is a significant dwell between the end of the DI of the high-reactivity fuel and the start of combustion.[2] There is a functional window of DI start-of-injection (SOI) timings that allows for successful RCCI combustion characterized by strong combustion phasing control as a function of DI timing. If the DI fuel is injected too early, the fuel and air mixture will become overly premixed and have little stratification in equivalence ratio or fuel composition and will approach HCCI with a binary fuel blend. On the contrary, as the DI timing approaches top dead center (TDC), high levels of equivalence ratio and fuel composition stratification will start to lead into mixing-controlled combustion for the DI portions of the fuel. Both physical and chemical properties of the fuels are expected to have an impact on this functional range.

Isolating the fuel effects with dual-fuel combustion modes can be challenging. The roles of chemical and physical fuel properties on the control of combustion phasing and duration, power density, low load operability, efficiency and emissions with RCCI have been investigated in recent studies, with recent review papers by Reitz and Duraisamy[3] and Paykani et al.[4] summarizing the progress that has been made to date. Most often these studies try to achieve the largest possible delta in fuel reactivity (e.g. gasoline and diesel fuel). Many of these fuel-related studies have investigated alternative fuels with high octane to increase power density by extending the upper load limit. For example, several studies have looked at ethanol's high antiknock properties.[5,6] Curran et al.[7] explored the role of an 85% ethanol–gasoline blend (E85) for the premixed fuel on extending the load range for RCCI in a multi-cylinder light-duty engine and found significant load increase compared to ethanol-free gasoline (E0). In a subsequent study, the role of high octane ethanol–gasoline blends in extending stable combustion over more of the light-duty drive cycle load range was also explored.[8] The

results of that study were presented in the context of increasing the drive cycle load range, which was shown to have improvements in fuel economy and lowered drive cycle emissions using vehicle system simulations. Other studies have investigated the use of methanol[9] and natural gas (methane).[10] DelVescovo et al.[11] investigated differences in physical and chemical properties of the premixed fuel by comparing iso-octane with syngas (50% H_2 and 50% CO) and methane, with *n*-heptane used for the DI fuel. That study found that with the gaseous fuels, similar efficiency and emissions to the baseline iso-octane case could be achieved by tailoring the DI strategy to match both the phasing and shape of the heat release.

Other studies have modified the reactivity of the DI fuel by adding cetane improvers. In Dempsey et al.,[12] the DI base fuel was the same 96-research octane number (RON) certification-grade gasoline as the premixed fuel with different levels of ethylhexyl nitrate (EHN) added to increase reactivity. Gasoline with 10%, 5%, and 2.5% EHN resulted in a measured cetane number of 62.6, 33.0, and 25.4, respectively, compared to 44.2 for the reference diesel fuel. The study found that diesel fuel allowed greater control authority over combustion phasing via DI timing than the doped gasoline, despite having a lower cetane number. The authors concluded that the lower volatility of diesel fuel led to greater fuel stratification and, therefore, appeared to be the dominant factor for combustion phasing when compared to cetane number. Chuahy et al.[13] examined the effects of physical properties of DI fuel in RCCI, with a focus on the effects of the distillation curve of the DI fuel. In that study, the distillation curve of #2 diesel was lowered by mixing it with a blend of 21% iso-octane and 79% *n*-heptane, which has a predicted cetane number similar to that of the diesel fuel but a much lower boiling point. Chuahy et al. found the boiling curve had large effect on combustion phasing in early-injection RCCI, but diminished effects as DI timing approached TDC and more mixing-limited combustion.

While many RCCI fuel combinations have been explored, there is a lack of fundamental understanding of which fuel properties (chemical or physical) are the most important, and in a wider scope, which properties are most desirable. A list of properties with potential importance is given for the fuels used in this study in Table 4. It is plausible to assume that based on their different roles in the combustion process and the different ways in which they are introduced to the combustion chamber, the desirable properties of the premixed and DI fuels may be considerably different. The most obviously desirable difference would that of autoignition tendency at the relevant conditions, which for lack of a precise definition is often referred to as "reactivity." This concept is often characterized by metrics such as octane number, cetane number, or HCCI index,[14] but none of these are universally applicable across the LTC spectrum.[15,16] As has also been shown in some of the literature mentioned thus far, physical properties such as boiling range can have a significant impact, and it can be imagined that other properties which affect the breakup and vaporization of sprays or the thermodynamic state of the charge may also play non-trivial roles. We are presently far from having the ability to take a list of fuel properties and make straightforward *a priori* predictions of operating range, efficiency, and emissions under RCCI operation.

The Co-Optimization of Fuels & Engines (Co-Optima) initiative is a collaborative effort sponsored by the US Department of Energy that involves nine national laboratories as well as industry. Co-Optima takes an integrated approach to improving efficiency and reducing emissions in vehicles by simultaneously researching engines, fuels, and marketplace strategies. A major part of achieving those goals is improving the understanding the effects of fuel properties on both conventional and advanced engine concepts. Within that context, this article represents part of a collaborative effort between Oak Ridge National Laboratory (ORNL) and Sandia National Laboratories (SNL) to improve the understanding of fuel effects on RCCI.

The all-metal, light-duty, multi-cylinder engine featured in this study will be used to derive conventional performance metrics such as efficiency, emissions, and pressure analysis under realistic operating conditions using production-viable hardware. In this sense, the ORNL engine will serve as a benchmark for the expected performance and the range of the experimental domain and will also be used to identify points of interest for further investigation at SNL using optical diagnostics. The optical, heavy-duty, single-cylinder engine at SNL will use both qualitative and quantitative imaging diagnostics to observe and quantify in-cylinder spatial and temporal development of fuel mixture preparation, ignition sites, and progression of combustion. The work at SNL will build on a previous study by Kokjohn et al.[17] that used fuel tracer fluorescence to visualize fuel reactivity stratification. The present study uses fuels with similar physical characteristics and a large difference in autoignition behavior to isolate the role of reactivity stratification and global reactivity on RCCI performance. This was accomplished by choosing primary reference fuels (PRFs) iso-octane and *n*-heptane to minimize the differences in the injection and mixing processes as different blends of the two fuels were investigated. Experimental results spanning RCCI operation from highly premixed dual-fuel LTC to dual-fuel mixing-controlled combustion are compared to results of RCCI with diesel fuel and HCCI with PRF blends. The transition points between combustion regimes are of interest in the larger context of understanding fuel properties and are linked to optical experiments that will help further illuminate the role of both the physical and chemical properties of fuels on RCCI control and load limit.[18]

Table 1. Specifications for the 2007 GM 1.9-L multi-cylinder diesel engine.

Number of cylinders	4
Bore (mm)	82.0
Stroke (mm)	90.4
Connecting rod length (mm)	145.4
Displacement (L)	1.91
Compression ratio (–)	16.5
IVO (°CA aTDC)	344
IVC (°CA aTDC)	−132
EVO (°CA aTDC)	116
EVC (°CA aTDC)	−340
Rated power (kW)	110
Rated torque (N m)	315

IVO: intake valve opening; CA: crank angle; aTDC: after top dead center; IVC: intake valve closing; EVO: exhaust valve opening; EVC: exhaust valve closing.

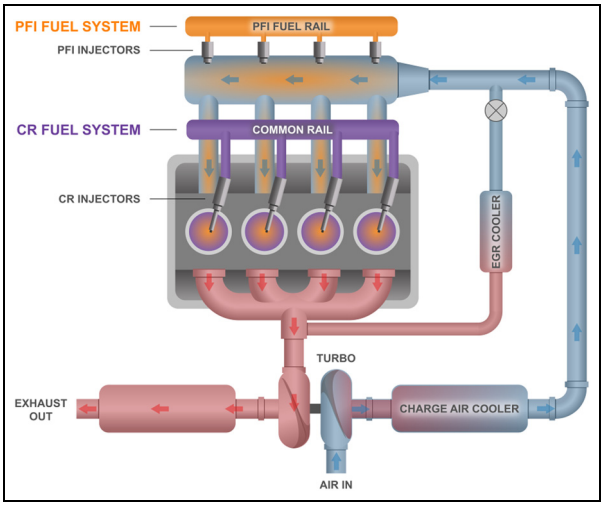

Figure 2. Diagram of the multi-cylinder GM 1.9-L engine. CR: common rail; EGR: exhaust gas recirculation; PFI: port fuel injection.

Methods

Experimental facilities

This study used a light-duty (automotive) 2007 GM 1.9-L 4-cylinder diesel engine, the specifications of which are provided in Table 1.

This engine is equipped with two fuel systems, as shown in Figure 2. The DI fuel is injected using the stock common-rail diesel fuel system, which is equipped with centrally mounted injectors whose specifications are given in Table 2. The on-engine portions of this system (high-pressure pump, fuel rail, and injectors) were kept in the stock configuration, but the supply and return were replaced with an in-house fuel delivery, conditioning, and measurement system. A port fuel injection (PFI) system was added to the engine by modifying the runners of the intake manifold to accept four port fuel injectors, described in Table 3. The spray of each port fuel injector was oriented as closely as possible to the back of an intake valve on the intake port without a swirl valve.

The stock variable-geometry turbocharger (VGT) was used, and the stock intercooler was replaced with an aftermarket charge air cooler with process water connections to allow for greater control over intake air temperature. Depending on the desired exhaust gas recirculation (EGR) flow rate, either a stock or aftermarket EGR cooler can be used with this engine. In either case, they are cooled via process water, and no EGR was used in this study. A variable swirl actuator (VSA) is located in the intake runner for each cylinder. These were set to the fully open condition for all cases shown in this study, creating the minimum possible swirl (swirl ratio ≈ 2).

Table 2. Common-rail direct injector specifications.

Model	Bosch CRI2.2
Number of holes	7
Hole size (μm)	140
Included spray angle (°)	148
Tip design	Mini-sac

Table 3. Port fuel injector specifications.

Model	Delphi Multec® 3.5 Extended tip PN 25380933
Number of holes	4
Separation angle (°)	22
Cone angle (°)	15

The stock engine control unit was replaced with a flexible data acquisition and control system from the National Instruments Powertrain Controls Group (formerly Drivven, Inc.) that allows for individual control of each injector and up to five injections per cycle for each DI injector. This system also controls all of the on-engine actuators, such as rail pressure, VGT position, VSA position, and EGR valve position.

In-cylinder pressure data were acquired with Kistler model 6125C pressure transducers, which were flush-mounted via the machined glow plug ports on each cylinder. Each transducer was connected to a Kistler model 5010 dual-mode amplifier, and the resulting signals were fed into the National Instruments system. Calculation, monitoring, and recording of combustion metrics were performed using Drivven combustion analysis software. High-speed data synced to the crankshaft encoder (in-cylinder pressure, injector current probes, etc.) were recorded for 300 consecutive cycles for all four cylinders, and low-frequency data (flow rates, temperatures, pressures, emissions, etc.) were recorded for 180 s at 2 Hz.

Emissions were measured with standard gaseous emission equipment sourced from California Analytical Instruments, Inc. Total unburned HC emissions in the exhaust were measured with a heated flame ionization detector and are reported on a C1 basis. Total NO_x ($NO + NO_2$) emissions in the exhaust were measured with a heated chemiluminescence detector. Both CO and CO_2 were measured with nondispersive infrared (NDIR) instruments: CO was measured in the exhaust

Table 4. Fuel properties.

Property	Fuel		
	Iso-octane (PRF100)	*n*-heptane (PRF0)	2007 Cert Diesel (ULSD)
Haltermann product number	HF3001	HF3002	HF0582
Formula	C_8H_{18}	C_7H_{16}	$C_xH_{(1.796x)}$[a,b]
Molecular weight (g/mol)	114.229[21]	100.202[21]	–
Purity (%)	99.88[a]	99.78[a]	–
Research octane number	100[22]	0[22]	–
Motor octane number	100[23]	0[23]	–
Cetane number	11–19[24]	53–54[24]	45.3[a]
Lower heating value (kJ/g)	44.3[25]	44.64[26]	42.6[a,b]
Stoichiometric AFR (g/g)	15.13[c]	15.08[c]	14.49[c]
Boiling point/range (°C)	99.2[21]	98.38[21]	171–366[a,b]
Density (kg/m^3) (20 °C)	691.9[21]	683.7[21]	849[a,b]
Vapor pressure (kPa) (25 °C)	6.5[21]	6.09[21]	0.13–1.3[b,d]
Heat of vaporization (kJ/kg) (25 °C/boiling point)	267/308[21,b]	317/365[21,b]	230–270[d]
Viscosity (mPa s) (25 °C)	0.289[27]	0.387[21]	1.95[a,b] (40 °C)
Surface tension (mN/m) (20 °C)	16.9[28]	18.5[29]	27–30[d]

PRF: primary reference fuel; ULSD: ultra-low-sulfur diesel; AFR: air-to-fuel ratio.
[a]Taken from Haltermann certificate of analysis.
[b]Units converted from source.
[c]Calculated using method described in Heywood.[25]
[d]Typical literature range.

in a dedicated instrument with simultaneous high and low ranges, and CO_2 was measured in both the exhaust and intake with separate instruments. Intake and exhaust O_2 were measured with separate instruments, both using a paramagnetic detector. The exhaust sample stream was maintained at 190 °C through heated filters and heated lines. Measurements of filter smoke number (FSN) were obtained with an AVL 415S smoke meter. FSN was found to be $\leqslant 0.01$ for all cases in this study and is therefore not reported for individual data points. Several studies have shown that FSN does not adequately measure the particulate matter produced by RCCI,[19] which tends to have a high volatile organic fraction. However, significant soot production was not expected at the conditions used here, and soot is not the focus of this work. Combustion noise was calculated using the approach shown in Shahlari et al.[20] using individual unfiltered pressure traces.

Experimental conditions

The properties of the three base fuels used in this study, iso-octane (2,2,4-trimethylpentane), *n*-heptane, and 2007 certification ultra-low-sulfur diesel (ULSD), are provided in Table 4. All fuels were sourced from Haltermann Solutions. The properties shown for iso-octane and *n*-heptane are derived from several literature sources and were not measured directly for the fuel used in the experiments. Most of the properties shown for the ULSD are taken from the certificate of analysis provided by Haltermann, and for the others, a typical literature range is provided, as noted. The PRF scale for gasoline-like fuels is based on iso-octane and *n*-heptane, which are defined as PRF100 and PRF0, respectively. The PRF scale is based on a volumetric combination of the PRFs and is used to define the RON[22] and motor octane number[23] of fuels being tested for knock resistance. A higher PRF number indicates greater resistance to autoignition or lower reactivity. It can be seen from the table that the lower heating value, stoichiometric air-to-fuel ratio, boiling point, and density for the PRFs are nearly identical, and the other physical properties listed are quite similar overall. Therefore, we would expect that replacing one PRF with the other or a blend of the two would not have a significant impact on the injection, vaporization, and mixing processes. The ULSD shown in Table 4 was used as a high-reactivity (DI) fuel, though its cetane number is lower than that of *n*-heptane. If this were the only difference between the two fuels, we would expect reactivity stratification to be marginally less effective with ULSD. However, its physical properties vary significantly from the PRFs. Most notable is the boiling range, which starts nearly 80 °C above the other fuels and occurs over a range of nearly 200 °C, rather than at a single temperature. This could have a significant impact on the distribution of different components of the fuel throughout the charge.[13] Note that the physical properties given here are at or near standard temperature and pressure and therefore may change significantly at combustion-relevant conditions. Also note that in the following tests, any PRFs or PRF blends used in the DI fuel system were blended with 350 ppm by mass of lubricity improver (Infineum R655) to protect the high-pressure pump and injectors. Details regarding the use of this lubricity improver with volatile fuels in this DI fuel system can be found in Dempsey et al.[30]

The experiments were organized into two sets of sweeps, both of which were performed at the same boundary conditions, as shown in Tables 5 and 6. For

Table 5. Experimental conditions for direct-injection start-of-injection sweeps.

Test	Fuel					
	PRF0/100, Rp70	PRF0/100, Rp80	PRF0/100, Rp90	PRF80/80, Rp80	PRF80, HCCI	D/PRF100, Rp70
DI fuel	PRF0	PRF0	PRF0	PRF80	–	ULSD
PFI fuel	PRF100	PRF100	PRF100	PRF80	PRF80	PRF100
Premix ratio (%)	70	80	90	80	100	70
Premix ϕ (–)	0.245	0.28	0.315	0.28	0.35	0.245
Global PRF	70	80	90	80	80	–
ΔPRF	100	100	100	0	N/A	–
DI SOI (°CA aTDC)	Start = −180 or stability limit End = PPRR limit (> 15 bar/°CA) or combustion efficiency limit (< 80%)					
DI fuel pressure (bar)	450					
Speed (r/min)	2000					
Global ϕ (–)	0.35 (No EGR)					
Fuel rate (J/cycle)	2100 (525/cylinder)					
BMEP (bar)	≈3.25					
T_{in} (C)	40					
P_{in} (bar)	≈1.04					
Air rate (g/s)	≈35 (8.75/cylinder)					

PRF: primary reference fuel; Rp: premix ratio; HCCI: homogeneous charge compression ignition; DI: direct injection; ULSD: ultra-low-sulfur diesel; PFI: port fuel injection; SOI: start of injection; CA: crank angle; aTDC: after top dead center; PPRR: peak pressure rise rate; EGR: exhaust gas recirculation; BMEP: brake mean effective pressure.
ϕ = fuel-air equivalence ratio.

Table 6. Experimental conditions for premix ratio sweeps.

Test	Fuel	
	PRF0/100, SOI55	PRF80/80, SOI55
DI fuel	PRF0	PRF80
PFI fuel	PRF100	PRF80
Premix ratio (%)	70–90	70–100
Premix ϕ (–)	0.245–0.315	0.245–0.35
Global PRF	70–90	80
ΔPRF	100	0
DI SOI (°CA aTDC)	−55	

PRF: primary reference fuel; SOI: start of injection; DI: direct injection; PFI: port fuel injection; CA: crank angle; aTDC: after top dead center.

all tests, the DI fuel rail pressure, engine speed, global equivalence ratio, intake temperature, and fueling rate were fixed, and fueling was specified on an energy basis. Intake pressure and air rate were set to achieve the desired equivalence ratio, and brake mean effective pressure (BMEP) varied with efficiency. No EGR was used, and combustion phasing was allowed to vary as the injection strategy was changed as shown in Figure 3. The set of fixed boundary conditions, developed in tandem with SNL to best match the linked optical engine experiments, represents a compromise that allows for a wide operating range of both premix ratio (Rp) and DI SOI with the given fuels in the ORNL engine while also allowing the thermodynamic state of the charge to be matched at a relevant point in the SNL engine. Further details on the matching between the two engines will be provided in the forthcoming optical study.

The first set of experiments, described in Table 5, consisted of sweeps of the DI SOI timing for various fuel combinations. For each test, the sweep started at either −180° CA after top dead center (aTDC) or the stability limit (ability to maintain combustion phasing within ±1° CA across all cylinders for the duration of data acquisition period) and ended when the peak pressure rise rate exceeded 15 bar/°CA or combustion efficiency fell below 80%. The first three tests all used neat PRFs, with PRF0 as the DI fuel and PRF100 as the PFI fuel, yielding a PRF difference between fuels (ΔPRF) of 100. These tests were performed at premix ratios of 70%, 80%, and 90%, resulting in a global PRF70, PRF80, and PRF90, respectively. Note that premix ratios reported here are on a mass basis, while PRF blends are defined on a volume basis. However, due to the nearly identical densities and heating values of the PRFs, reporting the premix ratio on a mass, energy, or volume basis would result in the same nominal global PRF. These first three tests, in which DI SOI was swept over a wide timing range at three different premix ratios, established the size of the relevant operating space of these boundary conditions. Also note that because the premix ratio was used to adjust the global PRF, the premixed equivalence ratio and the reactivity gradient also changed simultaneously. The global PRF could be changed at a fixed premix ratio by changing the PRF value in each fuel stream, but this would require the production of many fuel blends to perform the desired sweeps and was beyond the scope of this study.

Following the neat PRF tests, PRF80 blends were made from the base PRFs and used in both fuel streams. The engine was then fueled at a premix ratio of 80%. If we compare this test, named "PRF80/80, Rp80," to the previous test, "PRF0/100, Rp80," we would expect to have similar if not identical

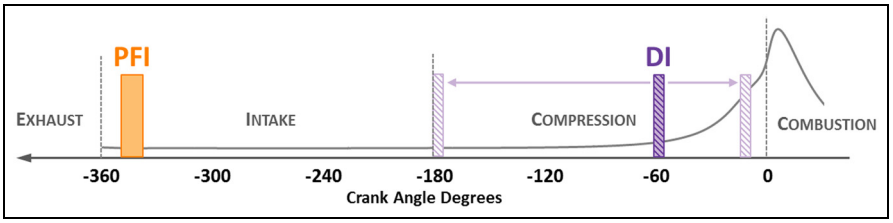

Figure 3. Reactivity-controlled compression ignition injection strategy used in this study: single port fuel injection (PFI) during early intake stroke and single direct injection (DI) with timing swept from bottom dead center to near top dead center of compression stroke.

equivalence ratio and temperature distributions up to the point of heat release, while at the same global PRF. The key difference between these two tests is that the case with neat PRFs will have reactivity stratification ($\Delta PRF = 100$), while the case with a single PRF80 fuel would not ($\Delta PRF = 0$). The PRF80 fuel was also used in a 100% premix ratio case to establish an HCCI baseline for the global PRF80. Note that up to this point, all cylinder-to-cylinder balancing was accomplished with duration multipliers on each of the DI injectors. These multipliers were limited to $\pm 20\%$ and were adjusted manually at each test point. When using these multipliers, the total flow rate of each fuel stream was maintained at the target level, but there was no direct measurement of the PFI or DI flow going into each cylinder. Therefore, while the premix ratio and global PRF for a given experimental sweep were held constant across the entire engine, there could be small differences between cylinders as required to maintain balance. For the HCCI case, where there is no DI, the data shown here are "unbalanced," as can be seen in the spread of combustion phasing in Figure 4. A repeat of this case was performed in which the cylinders were balanced with PFI multipliers and very similar average combustion phasing, performance, and emissions results were obtained. Figure 4 also shows two other cases at the same global PRF as the HCCI case, both with and without reactivity stratification. Although it was noted during the experiments that individual cylinders tended to be biased toward positive or negative balancing, there was considerable variation in the amount required as SOI and premix ratio were varied, and even at a fixed operating condition, the combustion phasing of each cylinder had a tendency to drift over time. This may be related to thermal cycling effects between cylinders and within the air handling and fuel injection systems, which appear to occur on timescales on the order of minutes. Further examination of these effects is outside the scope of this work, but will likely be of future interest.

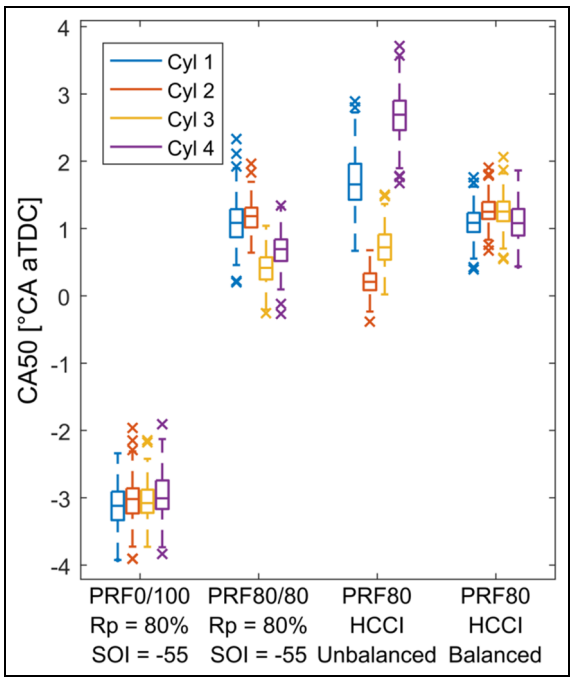

Figure 4. Box plots showing cylinder-to-cylinder variations in CA50. The extent of each box shows the interquartile range (IQR), the horizontal line inside the box shows the median, and the whiskers extend 1.5 × IQR from the box and cover $\approx 2.7\sigma$. aTDC: after top dead center; HCCI: homogeneous charge compression ignition; PRF: primary reference fuel; Rp: premix ratio; SOI: start of injection.

Finally, a DI SOI sweep was performed with ULSD as the DI fuel and PRF100 as the PFI fuel. The premix ratio was set to 70% to create the largest possible operating range in DI SOI space. This sweep was included primarily as a point of comparison and was not matched to the other sweeps in terms of global or local reactivity level, as the PRF of ULSD is not defined, and therefore neither are the global PRF or ΔPRF.

The second set of experiments, described in Table 6, consisted of sweeps of the premix ratio for two specific fuel combinations at a fixed DI SOI of $-55°$ CA aTDC, which is representative point within the RCCI regime from the first set of experiments. In the first sweep, with neat PRFs, the global PRF increased proportionally with premix ratio, which was swept from 70% to 90%. In the second sweep, in which both fuels were PRF80, the global PRF was fixed at 80% regardless of premix ratio. All other conditions were the same as in the previous set of experiments shown in Table 5. Similarly to the "PRF0/100, Rp80" and "PRF80/80, Rp80" cases already described, this configuration matches the equivalence ratio and temperature

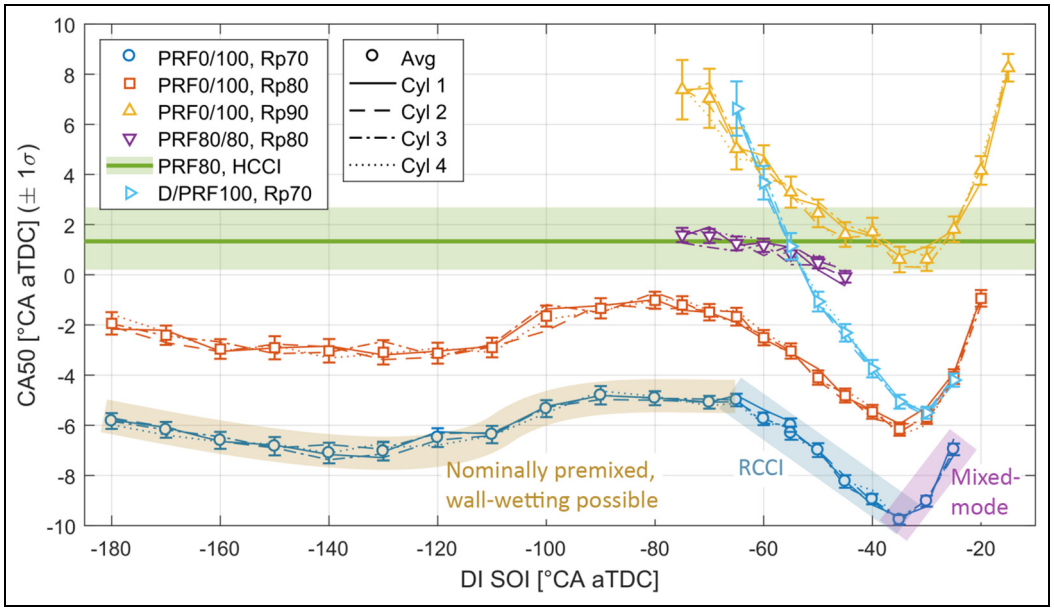

Figure 5. Crank angle at 50% of total heat release (CA50) versus direct-injection (DI) start of injection (SOI) for various fuel combinations. Line types represent the average CA50 for each cylinder, markers represent the average CA50 of all cylinders, error bars represent the average standard deviation of all cylinders, and the shaded region for the HCCI case represents the range of average CA50 between cylinders.
aTDC: after top dead center; HCCI: homogeneous charge compression ignition; PRF: primary reference fuel; Rp: premix ratio.

stratification between the two tests, allowing for the effects of reactivity stratification and global PRF to be isolated within the context of varying levels of equivalence ratio stratification.

Results and discussion

Injection timing sweeps

A plot of the response of the crank angle at 50% of total heat release (CA50) to changes in DI SOI for the various fuel combinations described in Table 5 is shown in Figure 5. Looking first at the "PRF0/100, Rp70" and "PRF0/100, Rp80" cases, we can identify three distinct regimes. Between −65° CA and −35° CA aTDC, there is a very linear negative relationship between CA50 and DI SOI that is characteristic of RCCI combustion. In this regime (RCCI regime), retarding DI SOI increases the level of reactivity stratification at the time of ignition by allowing less time for mixing of the two fuels, which results in both earlier combustion phasing and increased combustion duration. This can be seen clearly in Figure 6, which shows that the beginning of the main heat release advances with retarded DI SOI, potentially indicating that the reactivity of the first region to burn is increasing with stratification. Figure 6 also shows that while the slope on the tail of heat release varies, the end of heat release is virtually identical across the entire RCCI regime, suggesting that the reactivity of the last region to burn is similar regardless of DI SOI. Figure 5 shows that as DI SOI is further retarded, there is a sudden transition to a new regime in which CA50 retards rapidly. Comparing Figures 6 and 7, we can see that this change occurs due to the combustion of the DI fuel becoming increasingly limited by mixing time as DI SOI is retarded, eventually resulting in a bimodal heat release event. In this instance, we theorize that the first peak of the main heat release is a premixed burn of the DI fuel, which is followed by a coincident burn of diffusion-limited DI fuel and kinetically limited PFI fuel; therefore, we describe this as "mixed-mode" combustion. At the opposite end of the RCCI regime (early DI SOI), we may expect that the additional time allowed for mixing would reduce the level of reactivity stratification until a nearly homogeneous charge was reached, resulting in a CA50 that asymptotically approaches the HCCI value with advancing DI SOI. This regime could be considered "premixed." While a plateau in CA50 appears to be reached for DI SOI between −70° CA and −90° CA aTDC, we observe that further advance of DI SOI causes CA50 to advance, with a minimum reached around −130° CA to −140° CA aTDC. Further advancement of DI SOI beyond this point causes CA50 to retard again. This interesting and unexpected behavior may be caused by interaction between the DI spray and the cylinder liner and/or valves. This theory will be investigated in subsequent work, but it is not the focus of this work.

Comparing cases "PRF0/100, Rp70" and "PRF0/100, Rp80" in Figure 5, we observe that both have similar shape and features, with the primary difference being that Rp80 is retarded by 3°–4° CA, depending on DI SOI. This is expected, as the Rp80 case has both a higher global PRF and less of a reactivity gradient at a given DI SOI due to there being less DI fuel injected in

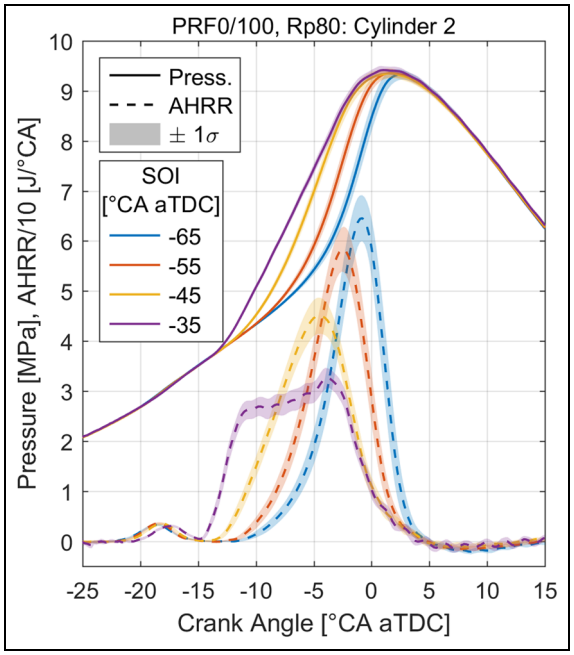

Figure 6. Ensemble average pressure and heat release traces with standard deviation bands for selected points in the reactivity-controlled compression ignition regime from the "PRF0/100, Rp80" case. Data are taken from cylinder 2.
AHRR: apparent heat release rate; aTDC: after top dead center; CA: crank angle; SOI: start of injection.

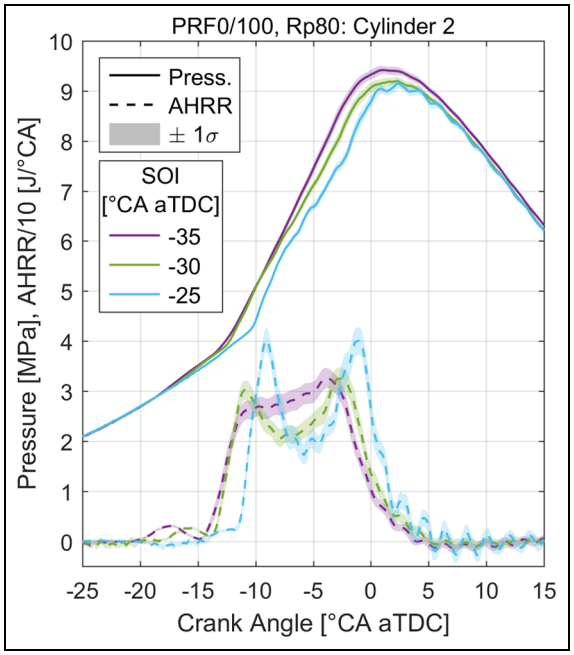

Figure 7. Ensemble average pressure and heat release traces with standard deviation bands for points in the mixed-mode regime from the "PRF0/100, Rp80" case. Data are taken from cylinder 2.
AHRR: apparent heat release rate; aTDC: after top dead center; CA: crank angle; SOI: start of injection.

that case. Increasing the premix ratio to 90%, as shown in the "PRF0/100, Rp90" case, causes a much larger retard in CA50, as well as increased cyclic variability. This indicates nonlinearity between CA50 and the premix ratio, which will be explored further in the second set of experiments. At Rp90, the neat PRFs could not be operated with DI SOI advanced beyond −75° CA aTDC due to low combustion stability (inability to maintain CA50 within ±1° CA for duration of data collection) at CA50 later than 8° CA aTDC.

Looking next to the single-fuel case "PRF80/80, Rp80," it is evident from Figure 5 that it has a much smaller operable DI SOI range than the cases with neat PRFs and that there is considerably less authority over CA50 as seen from the slope of the CA50 versus DI SOI curve. This case could not be run for DI SOI later than −45° CA aTDC due to excessive pressure rise rates, and it could not be run with balanced CA50 for DI SOI earlier than −75° CA aTDC because the DI fuel offered so little control and the limits on the duration multipliers (±20%) were reached. This case, which does not have reactivity stratification, had significantly retarded combustion phasing when compared to the equivalent case, "PRF0/100, Rp80," which did have reactivity stratification. If we compare the HCCI values to the "PRF80/80, Rp80" case, we observe that equivalence ratio stratification produces only a minor effect, especially in contrast to the effect of reactivity stratification. Note that "ϕ-sensitive" fuels can be used for combustion control with a single-fuel approach under boosted conditions[31] and that our experimental design intentionally removes this confounding variable by operating at essentially atmospheric intake pressure.

For the case with ULSD as the DI fuel, "D/PRF100, Rp70," several interesting features are present. The first is that while the combustion phasing was consistently retarded relative to the "PRF/100, Rp70" case due to the lower cetane number of ULSD relative to PRF0, the control over CA50 with DI SOI was much greater. It is presumed that the considerably different boiling range of ULSD plays a large part here, although the differences in the other physical properties cannot be ruled out. We also observe that the RCCI regime with ULSD is actually split into two subregimes, with a noticeable change in slope at −50° CA aTDC. Possible explanations for this change will be discussed in the following sections.

As a means of quantifying the control authority of SOI over CA50, robust linear least squares fitting of CA50 versus SOI was performed within the RCCI regime for each of the SOI sweeps, using data from all four cylinders. For each case, the average CA50 from each cylinder was fitted to a first-order polynomial with weights $\omega = 1/\sigma^2$ to reduce the impact of cylinders with higher variance. The fitting was performed using MATLAB's robust least squares algorithm with bisquare weights, which reduce the impact of points farther from the fitted line. The range of SOI used for each fit and the resulting slope and R^2 values are provided in Table 7. The ULSD case was binned into two

Table 7. Linear fit of CA50 versus SOI in the RCCI regime (slope shown with 95% confidence interval).

DI fuel	PFI fuel	Rp (%)	SOI range (°CA aTDC)	CA50/SOI (°CA/°CA)	R^2
PRF0	PRF100	70	−65 to −35	−0.166 ± 0.010	0.977
PRF0	PRF100	80	−65 to −35	−0.149 ± 0.009	0.978
PRF0	PRF100	90	−65 to −35	−0.140 ± 0.019	0.896
PRF80	PRF80	80	−65 to −45	−0.066 ± 0.022	0.673
ULSD	PRF100	70	−50 to −35	−0.268 ± 0.012	0.994
ULSD	PRF100	70	−65 to −50	−0.491 ± 0.030	0.989

DI: direct injection; PFI: port fuel injection; Rp: premix ratio; SOI: start of injection; CA: crank angle; aTDC: after top dead center; PRF: primary reference fuel; ULSD: ultra-low-sulfur diesel.

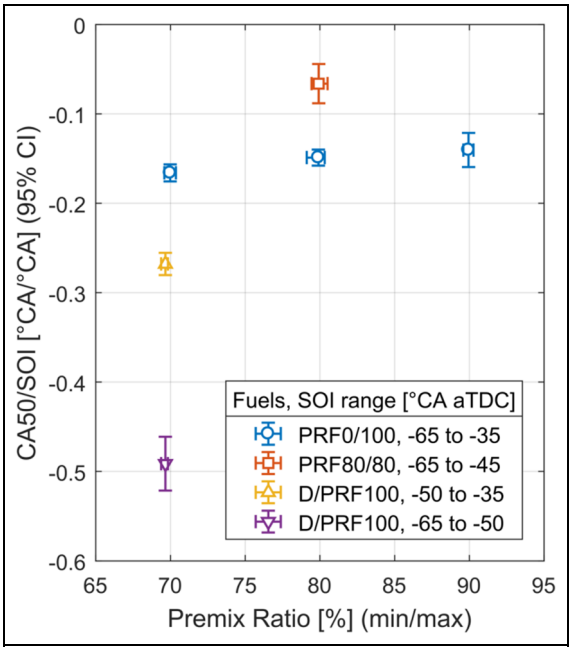

Figure 8. Slope of linear fit of the crank angle at 50% of total heat release (CA50) versus start of injection (SOI) in the reactivity-controlled compression ignition regime with 95% confidence interval (CI) plotted against premix ratio with minimum and maximum (min and max) values from each data set used for fitting.
aTDC: after top dead center; CA: crank angle; PRF: primary reference fuel.

regions, both of which included the point at −50° CA aTDC. The results are also plotted in Figure 8 as a function of premix ratio. All of the dual-fuel cases show a high correlation between CA50 and SOI, with $R^2 > \approx 0.9$, whereas the single-fuel PRF80 case had both a small slope and poor R^2 statistic, indicating that SOI offers limited influence over CA50 at these conditions and that a linear curve fit does not adequately capture the change in CA50 with respect to SOI. The addition of reactivity stratification increased the slope by over a factor of 2, but it is also seen that premix ratio had little influence within the range shown. This may indicate that for the PRF fuels, in which we expect physical differences to be negligible, the SOI control authority over CA50 is driven by ΔPRF, which is dictated by choice of PRF blend in each fuel stream, while the absolute CA50 at a given SOI is driven by the global PRF, which is dictated by the ratio of fuel streams.

It is also evident from the slope fitting results that the physical properties of the DI fuel may have a significant impact on the control authority of SOI over CA50. Despite the lower cetane number of ULSD relative to PRF0, the slope within the SOI range of −50° CA to −35° CA aTDC for the ULSD case was ≈1.6× higher than the equivalent PRF0 case at Rp70, and the slope within the SOI range of −65° CA to −50° CA aTDC was an additional ≈1.8× higher.

To further explore the control over heat release that is possible with the different fuel combinations shown in Table 5, the results of the SOI sweeps are plotted in terms of combustion duration versus combustion phasing in Figure 9. For each of the cases with the neat PRFs, a C-shaped operating region can be seen. The lower leg of this region corresponds to the RCCI regime, where retarding SOI causes CA50 (combustion phasing) to advance and CA25–75 (the number of crank angles between 25% and 75% of total heat release or combustion duration) to increase. When the transition to mixed-mode combustion occurs, further SOI retard leads to the upper leg of the C-shape, in which CA25–75 continues to increase, but CA50 quickly retards. By changing the premix ratio, the C-shape is translated to more retarded CA50 and longer CA25–75. The three cases with neat PRFs illustrate how reactivity stratification can offer a certain degree of independent control over combustion phasing and duration by changing the premix ratio and DI SOI. In contrast, the single-fuel PRF80 SOI sweep showed little ability to control CA50 and almost no ability to control CA25–75, and all of the points were clustered near the PRF80 HCCI condition. The "D/PRF100, Rp70" case gives a good example of how changing fuel properties can change the operating range in combustion duration versus phasing space. As previously discussed, this case is retarded relative to the equivalent PRF0 case but covers a greater range of combustion phasing. Within the RCCI regime, it also covers the same range of combustion duration as the equivalent PRF0 case. An interesting feature of this sweep is that the bottom leg of the shape curls up to longer combustion duration at more retarded CA50—this corresponds to the region with much steeper slope of CA50 versus SOI. Another

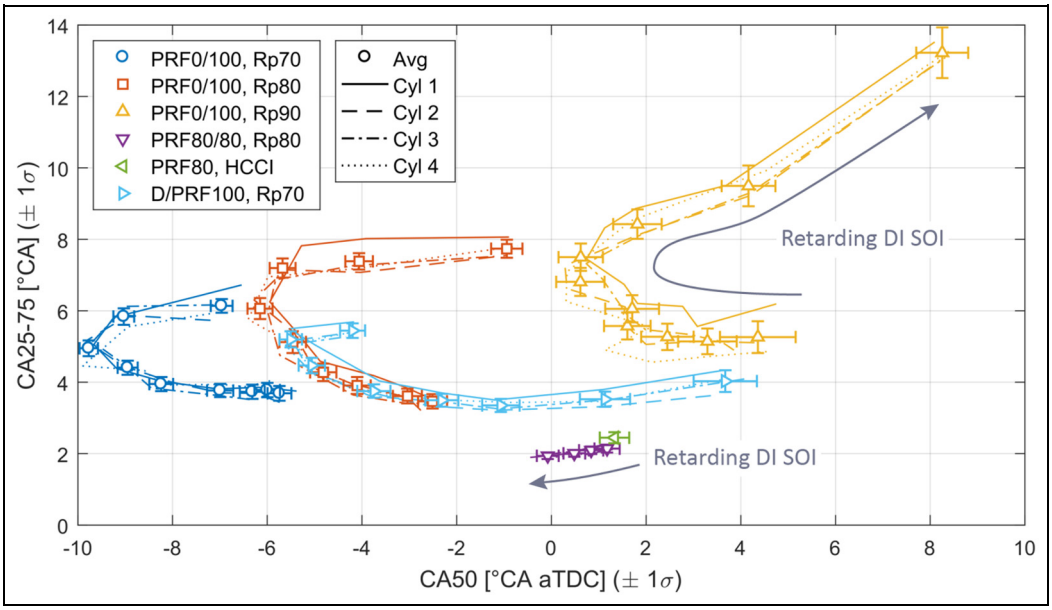

Figure 9. Combustion duration versus combustion phasing for start-of-injection (SOI) sweeps with various fuel combinations. Error bars in both directions represent the average of the standard deviation from all four cylinders. Data points at SOI before −65° CA after top dead center (aTDC) are excluded for clarity.
HCCI: homogeneous charge compression ignition; PRF: primary reference fuel; Rp: premix ratio.

aspect worth noting is that there is a region in which the case with ULSD overlaps the "PRF0/100, Rp80" case in terms of both duration and phasing. Where this overlap occurs, these two cases have very similar emissions and efficiency despite the difference in DI fuel composition. A study by DelVescovo et al.[11] has shown that premixed fuels with large differences in physical and chemical properties can be made to achieve similar efficiency and emissions if the DI strategy is modified to match the heat release shape (not merely CA50). While far from conclusive, the result presented here suggests that the same approach may apply when varying the properties of the DI fuel.

In each of the remaining plots in this section, only data with DI SOI $\geqslant -80°$ CA aTDC are shown. In Figure 10, combustion noise is plotted against DI SOI. For the PRF0/100, Rp70, and Rp80 cases, noise was very similar at early SOI and decreased as SOI was retarded and combustion duration increased, with the Rp80 case showing a larger noise reduction. The PRF0/100, Rp90 case had lower noise and higher variability at all SOI timings and showed less sensitivity to SOI retard. Both of the single-fuel PRF80 cases had similar noise levels, which were considerably higher than the other cases, and the PRF80/80, Rp80 case showed an increase in the noise as SOI was retarded, which coincided with a decrease in the combustion duration. At SOI timings later than −50° CA aTDC, the D/PRF100, Rp70 case followed a similar trend to the equivalent PRF0 case, albeit with slightly higher noise in the RCCI region. However, as SOI was advanced beyond −50° CA aTDC, a substantial decrease in the noise was observed, corresponding to the region in which the slope of CA50 versus SOI was much steeper.

Turning to the emission results, the brake-specific NO_x, CO, and HC are shown in Figures 11–13, respectively. Note that the vertical axis in each of these figures

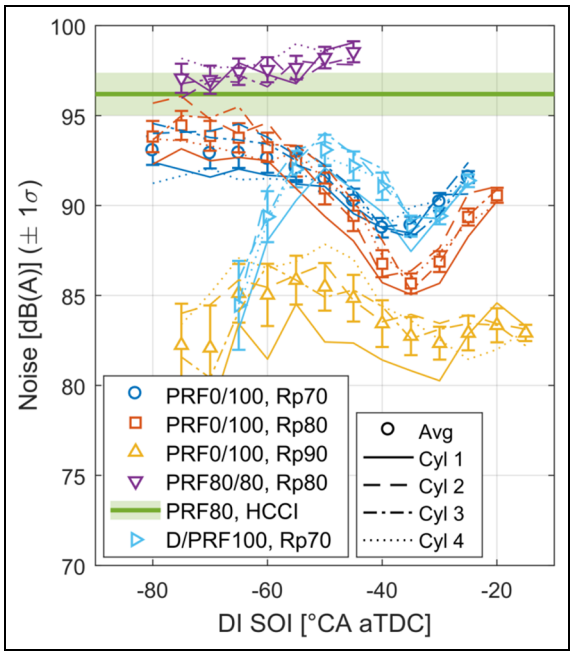

Figure 10. Noise versus direct-injection (DI) start of injection (SOI) for various fuel combinations. Error bars and shaded region represent one standard deviation.
aTDC: after top dead center; CA: crank angle; HCCI: homogeneous charge compression ignition; PRF: primary reference fuel; Rp: premix ratio.

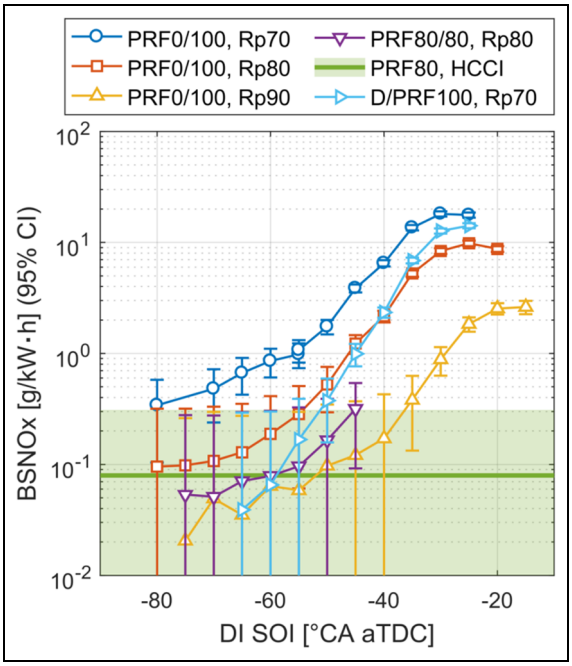

Figure 11. Brake-specific nitrogen oxides (BSNOx) versus direct-injection (DI) start-of-injection (SOI) timing for various fuel combinations. Error bars and shaded region represent 95% confidence interval (CI).
aTDC: after top dead center; CA: crank angle; PRF: primary reference fuel; Rp: premix ratio.

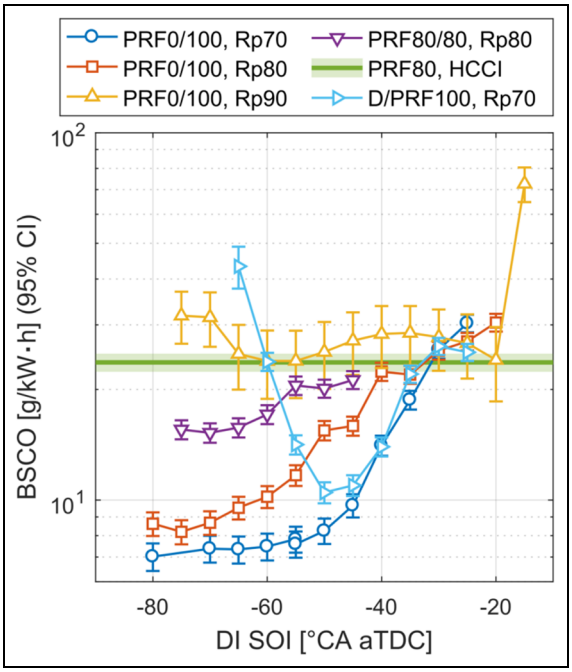

Figure 13. Brake-specific carbon monoxide (BSCO) versus direct-injection (DI) start-of-injection (SOI) timing for various fuel combinations. Error bars and shaded region represent 95% confidence interval (CI).
aTDC: after top dead center; CA: crank angle; PRF: primary reference fuel; Rp: premix ratio.

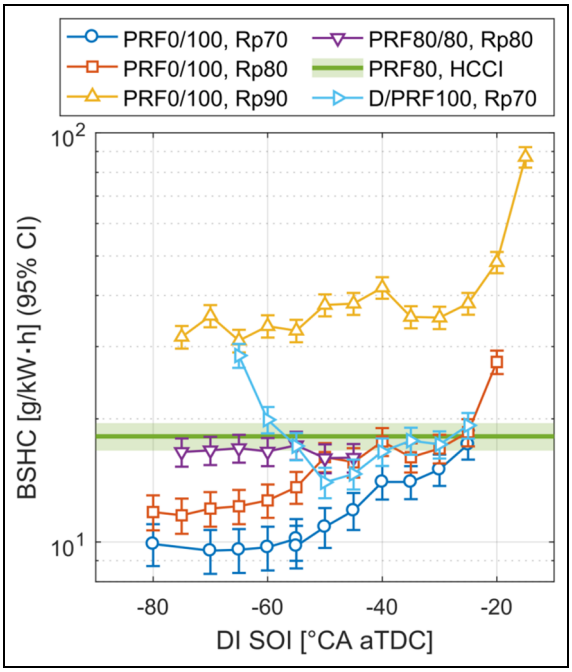

Figure 12. Brake-specific hydrocarbons (BSHC) versus direct-injection (DI) start-of-injection (SOI) timing for various fuel combinations. Error bars and shaded region represent 95% confidence interval (CI).
aTDC: after top dead center; CA: crank angle; PRF: primary reference fuel; Rp: premix ratio.

is shown in logarithmic scale due to the large range of emissions values encountered during the SOI sweeps. All of the cases follow a similar trend for NO_x, in which retarding DI SOI leads to substantial upward trend that plateaus in the mixed-mode region. For the neat PRFs, NO_x was observed to decrease with increased premix ratio, a trend which is linked to retarded combustion phasing at higher premix ratios. If Figure 11 is compared with the plot of CA50 versus DI SOI in Figure 5, there appears to be a relationship between delayed combustion phasing and decreased NO_x emissions as the premix ratio increases. This suggests that the volume of combusting gases that remains in near-stoichiometric proportions is reduced as Rp increases and SOI advances. The picture is more complicated for HC and CO. If we compare the neat PRF cases with one another, it appears that cases with greater stratification have lower HC and CO. However, as DI SOI is retarded, stratification levels increase, which corresponds to advancing CA50 and increasing HC and CO. This trend in HC and CO accelerates as DI SOI pushes into the mixed-mode regime, where there is a reversal in the CA50 trend. The reason for the lack of a consistent trend between CA50 and HC and CO is due to the inherent differences in increasing stratification by changing either the quantity or timing of the DI fuel. Increasing the quantity of the DI fuel at the same SOI increases the reactivity of the entire charge, both on a global and local basis, meaning that the reactivity of the least-reactive parts of the charge will have been increased, reducing the likelihood of unburned HCs remaining as the piston expands and the charge cools.

Decreasing the premix ratio also decreases the total fuel mass in the premixture available to be trapped in the crevice region, which is known to be a major source of unburned HCs in LTC strategies.[4] Alternatively, retarding the SOI with a given quantity of DI fuel stratifies the fuel without changing the global reactivity, meaning that the reactivity of the least-reactive part of the charge will have been decreased, thereby increasing the likelihood of incomplete combustion.

Comparing the equivalent dual- and single-fuel cases, we observe that the single-fuel cases achieved lower NO_x levels due to the relative lack of locally reactive regions which ignite early enough to burn at equivalence ratios that correspond with adiabatic flame temperature sufficient to produce NO_x. This lack of locally reactive regions, particularly in the "squish" region near the crevices where fuel is trapped during compression, also leads to much higher levels of HC and CO relative to the equivalent dual-fuel case. The diesel case had HC and CO between the values observed for the PRF0 cases at Rp70 and Rp80 at SOI later than −50° CA aTDC but showed a significant increase for both pollutants with more advanced SOI.

Combustion efficiency, which is derived from the emissions results, is shown in Figure 14. The single-fuel PRF80 cases all achieved a similar combustion efficiency of 90%–92%, and the PRF0/100, Rp70 case achieved the highest combustion efficiency at 96%. For the reasons already explained, increasing premix ratio and retarding SOI led to increased levels of HC and CO or reduced combustion efficiency. A significant decrease was seen for the PRF0/100, Rp90 case, which was shown above to have significantly retarded combustion phasing and higher cycle-to-cycle variability than the other PRF0 cases. The diesel case followed a similar trend to the PRF0/100 cases at Rp70 and Rp80 for SOI later than −50° CA aTDC, but suffered a significant drop in combustion efficiency at earlier SOI, which corresponds to the change in slope of CA50 observed in Figure 5.

BTE results are shown in Figure 15. The PRF0/100, Rp80 case achieved the highest BTE, followed closely by the single-fuel PRF80 cases. This finding can be understood by taking into account all of the results shown up to this point, which point to the PRF0/100, Rp80 case having the best compromise between combustion duration, combustion phasing, combustion efficiency, and heat transfer losses (which are expected to increase under ringing conditions[32] seen in single-fuel cases). Note that the PRF0 cases at Rp70 and Rp90 have very similar BTE at a given SOI, despite large differences in combustion efficiency. All of the cases with reactivity stratification show reduced BTE as SOI is retarded, with the exception of the earliest SOI for the diesel case, which had a similar trend reversal for combustion efficiency.

The trends for CA50, noise, emissions, and efficiency all indicate a trend reversal for the D/PRF100, Rp70 case at SOI earlier than −50° CA aTDC. One clue to the reason for this can be seen by examining the carbon balances shown in Figure 16. If there are assumed to be

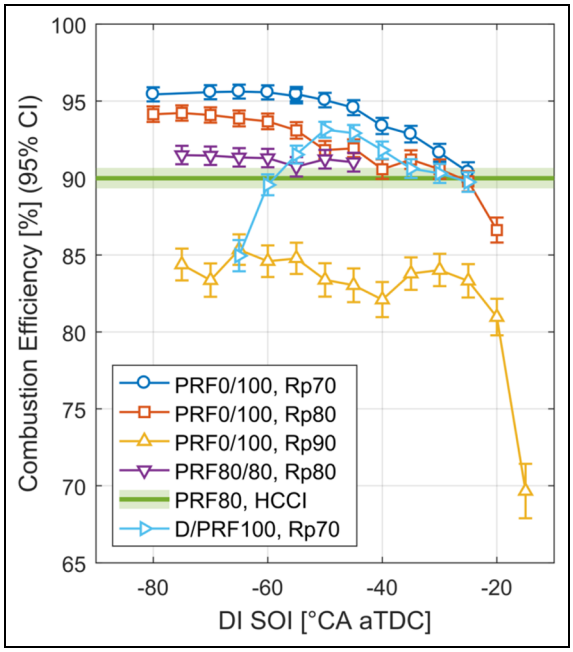

Figure 14. Combustion efficiency versus direct-injection (DI) start-of-injection (SOI) timing for various fuel combinations. Error bars and shaded region represent 95% confidence interval (CI).
aTDC: after top dead center; CA: crank angle; PRF: primary reference fuel; Rp: premix ratio.

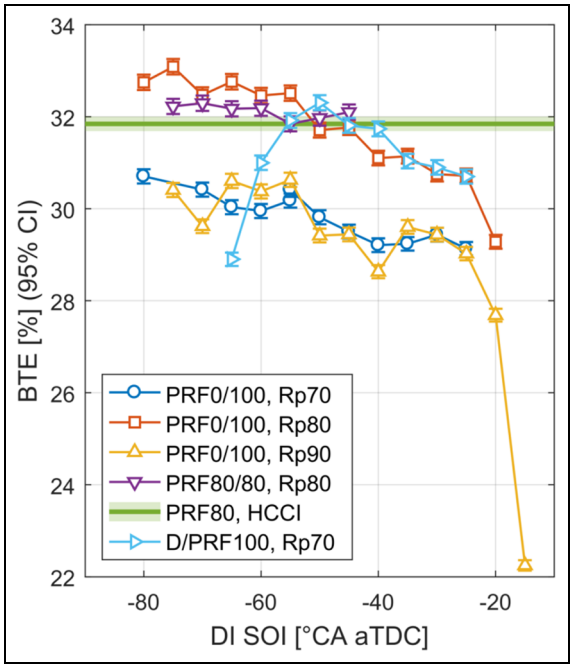

Figure 15. Brake thermal efficiency (BTE) versus direct-injection (DI) start-of-injection (SOI) timing for various fuel combinations. Error bars represent 95% confidence interval (CI).
aTDC: after top dead center; CA: crank angle; HCCI: homogeneous charge compression ignition; PRF: primary reference fuel; Rp: premix ratio.

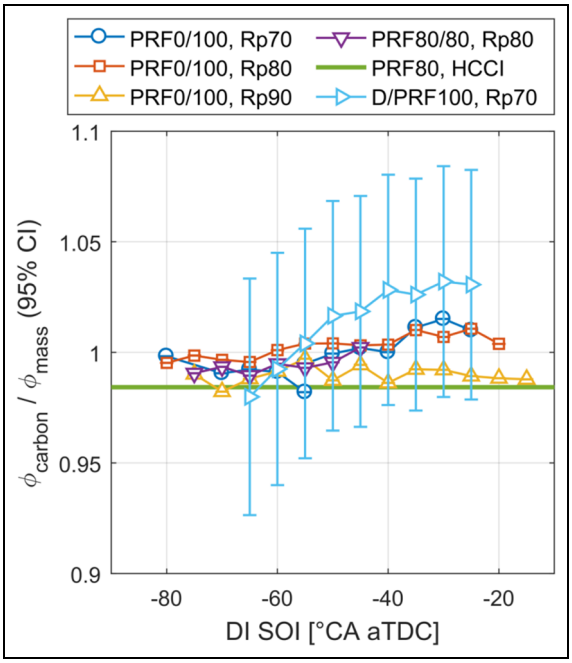

Figure 16. Carbon balance versus direct-injection (DI) start-of-injection (SOI) timing for various fuel combinations. Error bars represent 95% confidence interval (CI). Diesel case has been highlighted by removing error bars from other cases.
aTDC: after top dead center; CA: crank angle; HCCI: homogeneous charge compression ignition; PRF: primary reference fuel; Rp: premix ratio.

no air leaks between the air intake measurement point and the exhaust emissions measurement point, the ratio of carbon-based and mass-based equivalence ratios shown in Figure 16 can be interpreted as a ratio of fuel out to fuel in, as shown in equation (1). The subscripts in equation (1) refer to the method by which a given quantity was measured or derived—"stoich" refers to a stoichiometric balance based on the composition of the fuel, "carbon" refers to a carbon-atom balance based on measured exhaust species, and "mass" refers to measurements of the mass flow rates of fuel and air

$$\frac{\phi_{carbon}}{\phi_{mass}} = \frac{\frac{\left(air/fuel\right)_{stoich}}{\left(air/fuel\right)_{carbon}}}{\frac{\left(air/fuel\right)_{stoich}}{\left(air/fuel\right)_{mass}}} = \frac{\left(air/fuel\right)_{mass}}{\left(air/fuel\right)_{carbon}} = \frac{fuel_{carbon}}{fuel_{mass}} \quad (1)$$

Note that in Figure 16, the error bars, which were nearly identical in size for all data points, were removed from the PRF cases to improve clarity and highlight the diesel case. While all of the cases with direct-injected PRFs can be seen to cluster near a carbon ratio of unity with no significant trend as a function of SOI, the case with diesel shows a significant drop in carbon balance for SOI earlier than −50° CA aTDC. One potential explanation for this would be wall-wetting that results in the DI diesel fuel being absorbed into the oil film and therefore not measured in the exhaust. Due to the high volatility of PRFs, they may evaporate from the wall and therefore still participate in combustion and maintain the carbon balance.[33] As the diesel fuel is also the high-reactivity ignition source, it follows that cases in which significant portions of that fuel are being lost would suffer from retarded CA50 and degraded combustion performance.

Premix ratio sweeps

As described in Table 6, a second set of experiments was conducted on single- and dual-fuel cases at matched DI SOI to quantify the effects of premix ratio. Note that in the PRF0/100 case, changing the premix ratio affects the degree of equivalence ratio and reactivity stratification as well as the global PRF, while in the PRF80/80 case, changing premix ratio only changes the equivalence ratio stratification. Note that for all figures in this section, the 95% confidence intervals for premix ratio were not included because they were generally too small to be discernable and only served to reduce the clarity of the figure.

The response of CA50 to changes in premix ratio is shown in Figure 17. For the dual-fuel case, CA50 retarded linearly as premix ratio was increased from 70% to 77.5%, after which the CA50 retard was

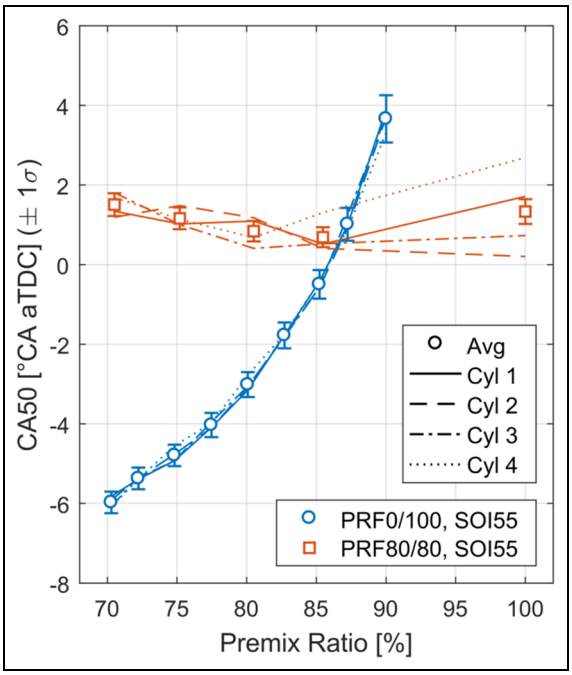

Figure 17. Combustion phasing versus premix ratio for two fuel combinations with matched physical properties at direct-injection (DI) start-of-injection (SOI) timing = −55° CA aTDC. Error bars represent the average of the standard deviation from all four cylinders.
aTDC: after top dead center; CA: crank angle; PRF: primary reference fuel; SOI: start of injection.

Table 8. Linear fit of combustion phasing (CA50) versus premix ratio (Rp) at direct-injection (DI) start-of-injection (SOI) timing = −55° CA after top dead center (slope shown with 95% confidence interval).

DI fuel	FI fuel	Rp range (%)	CA50/Rp (°CA, %)	R^2
PRF0	PRF100	70–75	0.252 ± 0.048	0.931
PRF0	PRF100	85–90	0.854 ± 0.078	0.983
PRF80	PRF80	70–90	-0.061 ± 0.032	0.479

DI: direct injection; PFI: port fuel injection; CA: crank angle; Rp: premix ratio.

accelerated with further increases in premix ratio. The single-fuel case, however, showed CA50 advancing slightly as premix ratio was increased from 70% to 85%. This indicates a possible inverted ϕ-sensitivity in which the additional charge cooling at lower premix ratios outweighs the natural tendency of high-ϕ regions to have shorter ignition delays. This effect has been explored as a control strategy in the literature.[34] The dual-fuel cases would presumably have the same amount of charge cooling at a given premix ratio, which indicates that the effect of reactivity stratification is significant enough to overcome the charge cooling and still give a large degree of control over CA50. Note that the single-fuel sweep also includes the unbalanced HCCI case shown in the previous section, which has a premix ratio of 100%.

To make a quantitative comparison of the control authority offered by premix ratio with the single- and dual-fuel cases, linear fits were performed to selected regions of the data, as shown in Table 8. Due to the obvious nonlinearity of the dual-fuel case, fits were performed on the first and last three points of the premix ratio sweep to establish a range of control authority. The fit for the single-fuel data excluded the HCCI condition. The results show that the magnitude of CA50 control via premix ratio is roughly 4–15 times greater at these nonboosted operating conditions when using two fuels with reactivity stratification.

In Figure 18, combustion duration is plotted against combustion phasing, allowing for a visualization of how the control of heat release evolves as premix ratio is changed. For the dual-fuel case, premix ratio is increasing in the direction of CA50 retard, and we observe that the initial increase in the premix ratio has marginal impact on combustion duration while retarding phasing. After the premix ratio passed 80%, the duration began to increase, as did the cylinder-to-cylinder variability. This increase in the combustion duration coincides with acceleration in the rate of phasing retard, which was also seen in Figure 17. For the single-fuel case, premix ratio is increasing in the direction of advancing CA50 and decreasing CA25–75, though it can be difficult to discern due to the tight clustering of the points. The exception to this trend is the HCCI condition, which has the most retarded CA50 and longest CA25–75 of the single-fuel Rp sweep. Although the absolute change in combustion duration and phasing is small for the single-fuel case, it is worth noting that the trend is in the opposite direction of the dual-fuel case.

Pressure and heat release traces for the dual- and single-fuel cases are shown in Figures 19 and 20, respectively. Looking first to the dual-fuel case, we can compare the control over heat release offered by premix ratio to that offered by DI SOI, as shown previously in Figure 6. Whereas changing SOI at a fixed premix ratio was seen to have little effect on low-temperature heat release (LTHR) and to advance the start of heat release while leaving the end in place, increasing premix ratio decreased LTHR while retarding both the start and end of main heat release. At higher premix ratios, the end of main heat release began to occur later than TDC, leading it to retard faster than the start of main heat release, which increased combustion duration. In contrast, the single-fuel case showed little ability to control phasing or duration, resulting in high peak heat release rates and indications of ringing on the expansion side of the pressure trace.

The calculated combustion noise from both premix ratio sweeps is plotted in Figure 21. The trends follow directly from the observations of peak heat release rate and combustion duration, which are inversely related for a fixed quantity of energy release. For the dual-fuel case, noise was essentially flat at lower premix ratios where duration was constant, and noise then began to decrease as premix ratio and combustion duration increased. The noise for the single-fuel case was 4.5 dB higher than the dual-fuel case at 70% Rp and increased slightly with increasing premix ratio and decreasing combustion duration.

The emissions results for the premix ratio sweeps are shown in Figures 22–24. NO_x for the single-fuel case was uniformly low, whereas the dual-fuel case had brake-specific NO_x near 1 g/(kW h) at 70% premix ratio, which decreased with increasing premix ratio until reaching the single-fuel value at a premix ratio of 85%. This trend mirrors that of combustion phasing in Figure 17. Both HC and CO increased dramatically with premix ratio under dual-fuel operation, agreeing with the observation from the first set of experiments and with the expectation that an overall less-reactive charge will have a larger amount of unburned and partially oxidized fuel. Under single-fuel operation, measured HC was largely unaffected by premix ratio and was at a level slightly higher than the dual-fuel case with equivalent global reactivity (PRF80). Similarly,

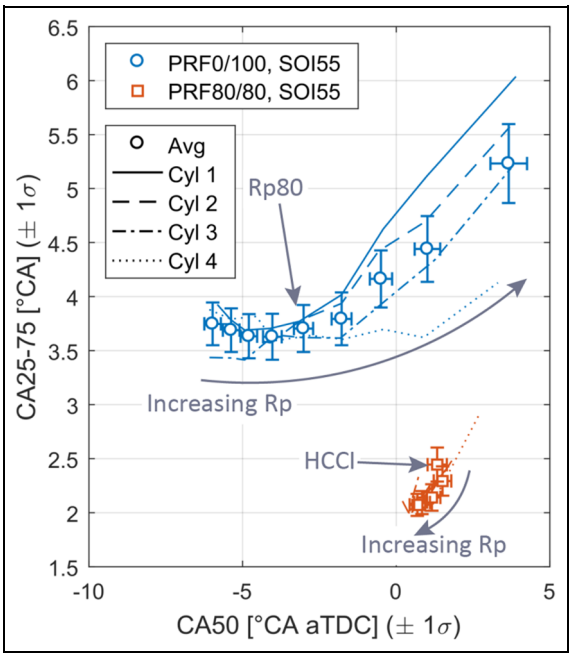

Figure 18. Combustion duration versus combustion phasing for premix ratio sweeps of two fuel combinations with matched physical properties at direct-injection (DI) start-of-injection (SOI) timing = −55° CA aTDC. Error bars in both directions represent the average of the standard deviation from all four cylinders.
aTDC: after top dead center; CA: crank angle; PRF: primary reference fuel; Rp: premix ratio; SOI: start of injection.

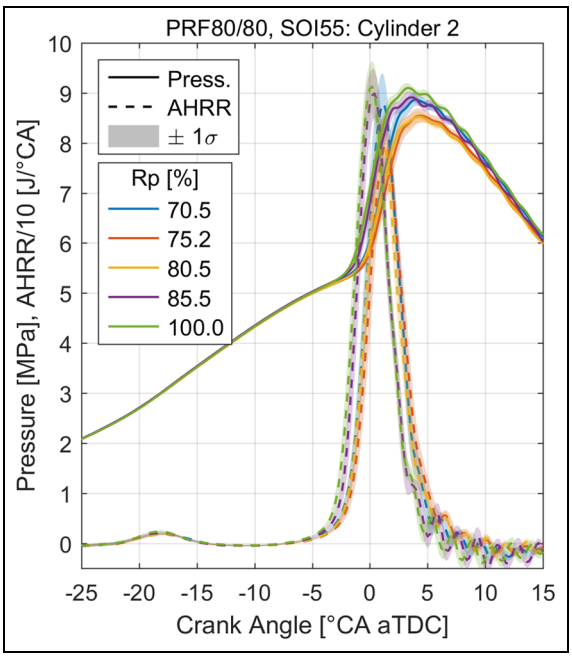

Figure 20. Ensemble average pressure and heat release traces with standard deviation bands for selected points from the PRF80/80, SOI55 case. Data are taken from cylinder 2.
AHRR: apparent heat release rate; aTDC: after top dead center; CA: crank angle; PRF: primary reference fuel; Rp: premix ratio; SOI: start of injection.

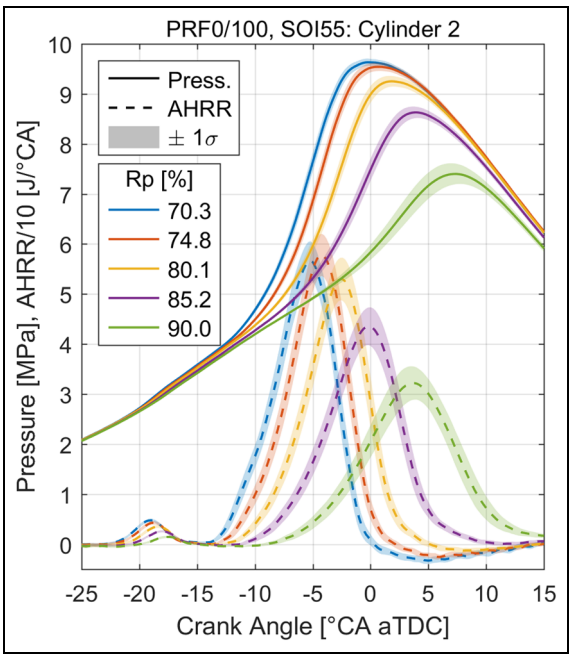

Figure 19. Ensemble average pressure and heat release traces with standard deviation bands for selected points from the PRF0/100, SOI55 case. Data are taken from cylinder 2.
AHRR: apparent heat release rate; aTDC: after top dead center; CA: crank angle; PRF: primary reference fuel; Rp: premix ratio; SOI: start of injection.

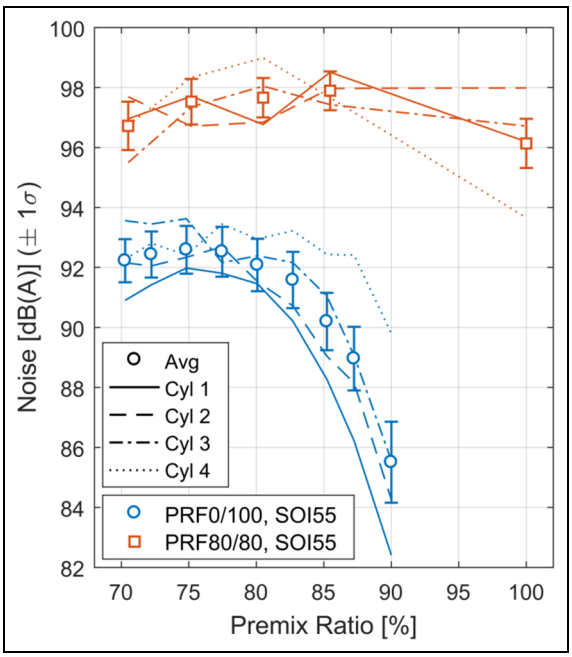

Figure 21. Noise versus premix ratio for two fuel combinations with matched physical properties at direct-injection (DI) start-of-injection (SOI) timing = −55° CA aTDC. Error bars represent the average of the standard deviation from all four cylinders.
PRF: primary reference fuel; SOI: start of injection.

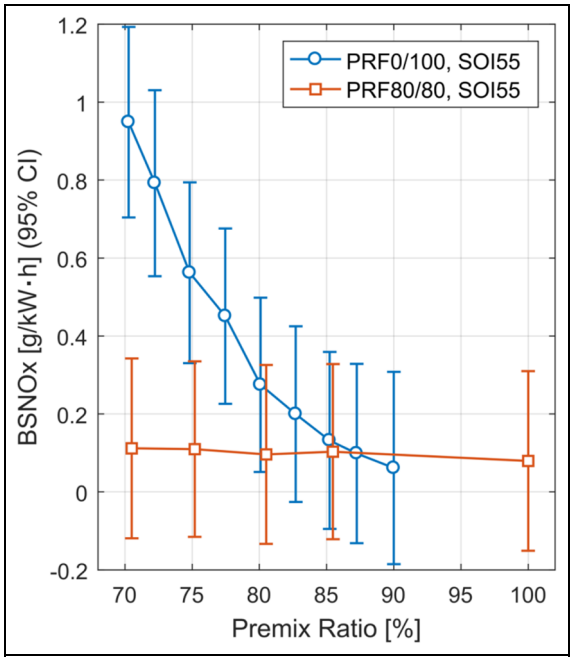

Figure 22. Brake-specific nitrogen oxides (BSNOx) versus premix ratio for two fuel combinations with matched physical properties at direct-injection (DI) start-of-injection (SOI) timing = −55° CA aTDC. Error bars represent 95% confidence interval (CI).
PRF: primary reference fuel; SOI: start of injection.

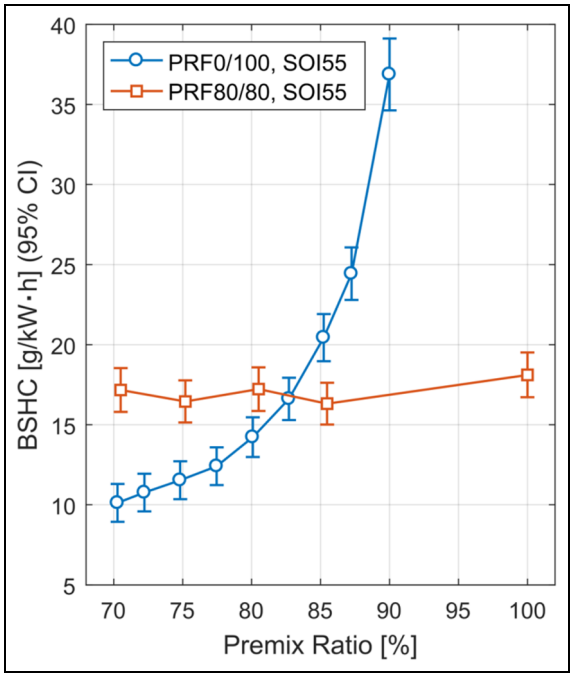

Figure 23. Brake-specific hydrocarbons (BSHC) versus premix ratio for two fuel combinations with matched physical properties at direct-injection (DI) start-of-injection (SOI) timing = −55° CA aTDC. Error bars represent 95% confidence interval (CI).
PRF: primary reference fuel; SOI: start of injection.

single-fuel CO levels were in the middle of the range encountered under dual-fuel operation, and there was

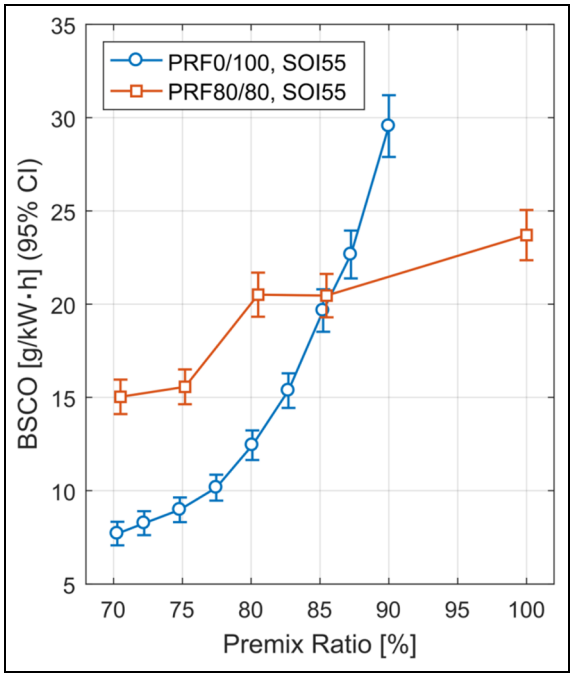

Figure 24. Brake-specific CO (BSCO) versus premix ratio for two fuel combinations with matched physical properties at direct-injection (DI) start-of-injection (SOI) timing = −55° CA aTDC. Error bars represent 95% confidence interval (CI).
PRF: primary reference fuel; SOI: start of injection.

an increase in the CO at a premix ratio of 80%, though it is unclear why this occurred.

The HC and CO results were used to calculate combustion efficiency, which is shown in Figure 25. At a premix ratio of 70%, the combustion efficiency of the dual-fuel case is higher by 4% absolute, but this drops quickly for the dual-fuel case as premix ratio is increased, while varying by less than 1% for the single-fuel case.

BTE is shown in Figure 26. Despite the continual decrease in combustion efficiency, BTE increases rapidly for the dual-fuel case as premix ratio is increased up to 80%, at which point, the trend reverses. This indicates that gains due to more optimal combustion phasing initially outweigh the losses due to unreacted HC and CO, but this is no longer the case once the combustion duration starts to increase. The single-fuel case has fairly uniform BTE, and despite having shorter combustion duration and CA50 near TDC, it is exceeded by the highest values from the dual-fuel case due to differences in combustion efficiency and potentially higher heat transfer resulting from ringing in the single-fuel case.[32]

Conclusion

Experiments were conducted at fixed boundary conditions with the neat and blended PRFs iso-octane and *n*-heptane to isolate the effect of reactivity stratification from that of equivalence ratio stratification within the

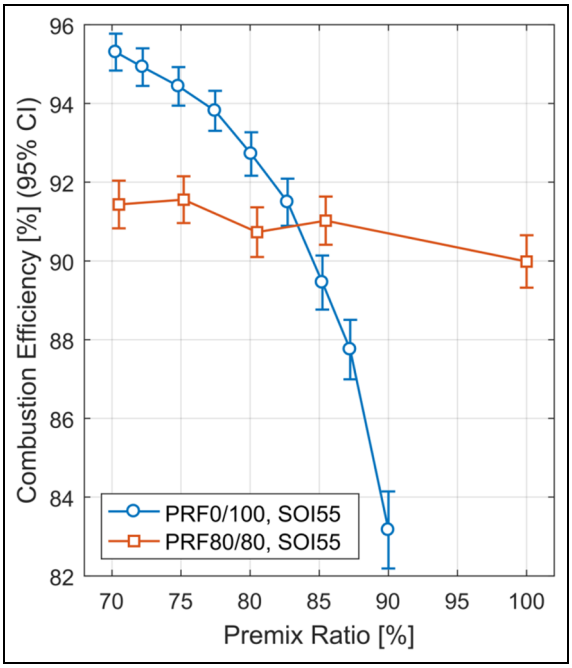

Figure 25. Combustion efficiency versus premix ratio for two fuel combinations with matched physical properties at direct-injection (DI) start-of-injection (SOI) timing = −55° CA aTDC. Error bars represent 95% confidence interval (CI).
PRF: primary reference fuel; SOI: start of injection.

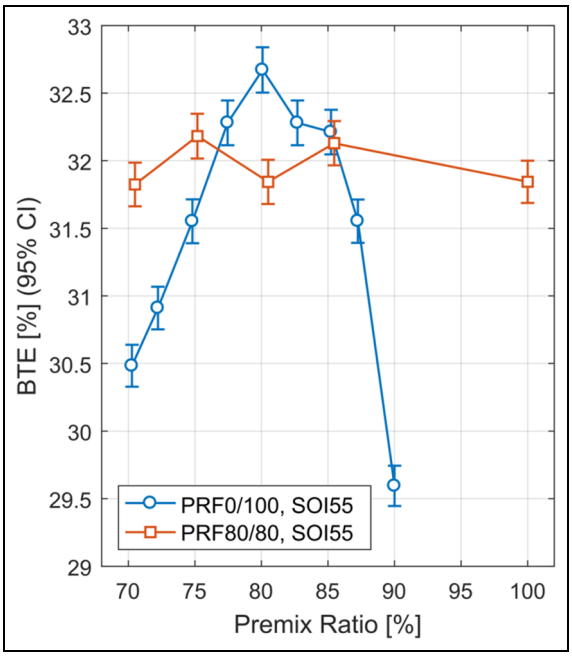

Figure 26. Brake thermal efficiency (BTE) versus premix ratio for two fuel combinations with matched physical properties at direct-injection (DI) start-of-injection (SOI) timing = −55° CA aTDC. Error bars represent 95% confidence interval (CI).
PRF: primary reference fuel; SOI: start of injection.

range of injection timings encompassing RCCI operation. A limited set of experiments were also performed with diesel as the high-reactivity fuel for a point of comparison with a representative distillate fuel. For sweeps of high-reactivity fuel SOI timing with matched premix ratio, equivalence ratio stratification, and global PRF, the addition of reactivity stratification resulted in the following:

- Three times greater combustion phasing control authority.
- More than 4 dB lower combustion noise and the ability to control noise with SOI thus reducing noise by an additional 8 dB.
- Increased brake-specific NO_x at a given SOI, but lower HC and CO emissions.
- Marginally increased BTE.

For sweeps of premix ratio with matched equivalence ratio stratification and matched SOI timing within the range of favorable control authority for RCCI, the addition of reactivity stratification and global PRF control resulted in the following:

- Four to 15 times greater combustion phasing control authority, depending on global PRF.
- More than 4 dB lower combustion noise and the ability to control noise with premix ratio thus reducing noise by an additional 7 dB over the range tested.
- Increased brake-specific NO_x and decreased HC and CO emissions at matched global PRF and the ability to change all three by changing PRF.
- Higher BTE within a range of global PRFs.

By adjusting both SOI and premix ratio, the possibility of reactivity stratification offered by a dual-fuel approach enables independent control of combustion phasing and duration across a much larger space than can be achieved with a single fuel under these non-boosted operating conditions. Experiments with diesel fuel also offered a glimpse at the potential to take advantage of the physical properties of the direct-injected fuel to influence the RCCI combustion process. The work presented here also points to several potential future directions on the multi-cylinder engine as follows:

- Evaluation of additional PRF blends to improve the understanding of ΔPRF on control authority.
- Investigation of the effects of injection pressure on control authority with both PRFs and real fuels.
- Performing similar experiments as shown here under boosted conditions to probe interactions between reactivity stratification and ϕ-sensitivity.
- Development of fuel blends with similar reactivity but different boiling curves, or variations in other physical properties of interest.

Nomenclature

ΔPRF	PRF difference between fuels
ϕ	fuel-air equivalence ratio
°CA	Crank angle degrees
AHRR	apparent heat release rate
aTDC	after top dead center
BDC	bottom dead center
BSCO	Brake-specific CO
BSHC	Brake-specific HC
$BSNO_x$	brake-specific NO_x
BTE	brake thermal efficiency
CA25–75	number of crank angles between 25% and 75% of total heat release (combustion duration)
CA50	crank angle at 50% of total heat release (combustion phasing)
CO	carbon monoxide
Co-Optima	Co-Optimization of Fuels & Engines (initiative)
DI	direct injection
EGR	exhaust gas recirculation
EHN	ethyl-hexyl nitrate
EVC	exhaust valve closing
EVO	exhaust valve opening
FSN	filter smoke number
HC	hydrocarbons
HCCI	homogeneous charge compression ignition
IR	infrared
IVC	intake valve closing
IVO	intake valve opening
LTC	low-temperature combustion
LTHR	low-temperature heat release
NO_x	nitrogen oxides
ORNL	Oak Ridge National Laboratory
PFI	port fuel injection
PRF	primary reference fuel
RCCI	reactivity-controlled compression ignition
RON	research octane number
Rp	premix ratio
SNL	Sandia National Laboratories
SOI	start of injection
TDC	top dead center
ULSD	ultra-low-sulfur diesel
VGT	variable geometry turbocharger
VSA	variable swirl actuator

Acknowledgements

This research used resources at the National Transportation Research Center, a DOE Office of Energy Efficiency and Renewable Energy User Facility operated by the Oak Ridge National Laboratory.

Declaration of conflicting interests

The author(s) declared no potential conflicts of interest with respect to the research, authorship, and/or publication of this article.

Funding

The author(s) disclosed receipt of the following financial support for the research, authorship, and/or publication of this article: This research was conducted as part of the Co-Optimization of Fuels & Engines (Co-Optima) initiative sponsored by the US Department of Energy (DOE) Office of Energy Efficiency and Renewable Energy (EERE), Bioenergy Technologies and Vehicle Technologies Offices. Co-Optima is a collaborative project of multiple National Laboratories initiated to simultaneously investigate advanced engine designs and enabling fuel properties.

References

1. Dempsey AB, Curran SJ and Wagner RM. A perspective on the range of gasoline compression ignition combustion strategies for high engine efficiency and low NOx and soot emissions: effects of in-cylinder fuel stratification. *Int J Engine Res* 2016; 17: 897–917.
2. Kokjohn S, Hanson R, Splitter D and Reitz R. Fuel reactivity controlled compression ignition (RCCI): a pathway to controlled high-efficiency clean combustion. *Int J Engine Res* 2011; 12: 209–226.
3. Reitz RD and Duraisamy G. Review of high efficiency and clean reactivity controlled compression ignition (RCCI) combustion in internal combustion engines. *Prog Energ Combust* 2015; 46: 12–71.
4. Paykani A, Kakaee A-H, Rahnama P and Reitz RD. Progress and recent trends in reactivity-controlled compression ignition engines. *Int J Engine Res* 2016; 17: 481–524.
5. Splitter D, Hanson R, Kokjohn S and Reitz RD. Reactivity controlled compression ignition (RCCI) heavy-duty engine operation at mid-and high-loads with conventional and alternative fuels. SAE technical paper 2011-01-0363, 2011.
6. Han X, Zheng M and Tjong J. Clean combustion enabling with ethanol on a dual-fuel compression ignition engine. *Int J Engine Res* 2015; 16: 639–651.
7. Curran S, Hanson R and Wagner R. Effect of E85 on RCCI performance and emissions on a multi-cylinder light-duty diesel engine. SAE technical paper 2012-01-0376, 2012.
8. Curran S, Gao Z and Wagner R. Reactivity controlled compression ignition drive cycle emissions and fuel economy estimations using vehicle systems simulations with E30 and ULSD. *SAE Int J Engine* 2014; 7: 902–912.
9. Dempsey AB, Walker NR and Reitz RD. Effect of piston bowl geometry on dual fuel reactivity controlled compression ignition (RCCI) in a light-duty engine operated with gasoline/diesel and methanol/diesel. *SAE Int J Engine* 2013; 6: 78–100.
10. Nieman DE, Dempsey AB and Reitz RD. Heavy-duty RCCI operation using natural gas and diesel. *SAE Int J Engine* 2012; 5: 270–285.
11. DelVescovo D, Kokjohn S and Reitz R. The effects of charge preparation, fuel stratification, and premixed fuel chemistry on reactivity controlled compression ignition (RCCI) combustion. *SAE Int J Engine* 2017; 10(4): 1491–1505.
12. Dempsey AB, Curran S and Reitz RD. Characterization of reactivity controlled compression ignition (RCCI) using premixed gasoline and direct-injected gasoline with a cetane improver on a multi-cylinder engine. *SAE Int J Engine* 2015; 8: 859–877.
13. Chuahy F, Ra Y and Kokjohn S. Effects of the direct-injected fuel physical properties under early and late reactivity con-trolled compression ignition (RCCI) combustion. In: *Proceedings of the ILASS Americas 27th annual conference on liquid atomization and spray systems*, Raleigh, NC, May 2015. Retrieved from http://www.ilass.org/2/recent-papers-form.html

14. Shibata G and Urushihara T. Auto-ignition characteristics of hydrocarbons and development of HCCI fuel index. SAE technical paper 2007-01-0220, 2007.
15. Kalghatgi GT. Auto-ignition quality of practical fuels and implications for fuel requirements of future SI and HCCI engines. SAE technical paper 2005-01-0239, 2005.
16. Richards P. *Automotive fuels reference book*. 3rd ed. Warrendale, PA: SAE International, 2014.
17. Kokjohn S, Reitz RD, Splitter D and Musculus M. Investigation of fuel reactivity stratification for controlling PCI heat-release rates using high-speed chemiluminescence imaging and fuel tracer fluorescence. *SAE Int J Engine* 2012; 5: 248–269.
18. Roberts G, Rousselle CM, Musculus M, Wissink M, Curran S and Eagle E. RCCI combustion regime transitions in a single-cylinder optical engine and a multi-cylinder metal engine. *SAE Int J Engine* 2017; 10(5): 2017.
19. Storey J, Curran S, Dempsey A, Lewis S, Ryan Walker N, Reitz R and Wright C. The contribution of lubricant to the formation of particulate matter with reactivity controlled compression ignition in light-duty diesel engines. *Emiss Control Sci Technol* 2015; 1: 64–79.
20. Shahlari AJ, Hocking C, Kurtz E and Ghandhi J. Comparison of compression ignition engine noise metrics in low-temperature combustion regimes. *SAE Int J Engine* 2013; 6: 541–552.
21. Haynes WM. *CRC handbook of chemistry and physics* (Internet version 2017). 97th ed. Boca Raton, FL: CRC Press/Taylor & Francis, 2017.
22. ASTM D2699-16e1. Standard test Method for research octane number of spark-ignition engine fuel. West Conshohocken, PA: ASTM International, 2016. Retrieved from www.astm.org
23. ASTM D2700-16a. Standard test method for motor octane number of spark-ignition engine fuel. West Conshohocken, PA: ASTM International, 2016. Retrieved from www.astm.org
24. Yanowitz J, Ratcliff MA, McCormick RL, Taylor JD and Murphy MJ. *Compendium of experimental cetane numbers*. Golden, CO: National Renewable Energy Laboratory, 2014.
25. Heywood J. *Internal combustion engine fundamentals*. New York: McGraw-Hill Education, 1988.
26. Szybist JP, Chakravathy K and Daw CS. Analysis of the impact of selected fuel thermochemical properties on internal combustion engine efficiency. *Energ Fuel* 2012; 26: 2798–2810.
27. Padua A, Fareleira J, Calado J and Wakeham W. Density and viscosity measurements of 2,2,4-trimethylpentane (isooctane) from 198 K to 348 K and up to 100 MPa. *J Chem Eng Data* 1996; 41: 1488–1494.
28. Kao Y-C and Tu C-H. Densities, viscosities, refractive indexes, and surface tensions for binary and ternary mixtures of tetrahydofuran, 2-propanol, and 2,2,4-trimethylpentane. *J Chem Thermodyn* 2011; 43: 216–226.
29. Rolo LI, Caco AI, Queimada AJ, Marrucho IM and Coutinho JA. Surface tension of heptane, decane, hexadecane, eicosane, and some of their binary mixtures. *J Chem Eng Data* 2002; 47: 1442–1445.
30. Dempsey AB, Curran S, Wagner R and Cannella W. Effect of premixed fuel preparation for partially premixed combustion with a low octane gasoline on a light-duty multicylinder compression ignition engine. *J Eng Gas Turb Power* 2015; 137: 111506.
31. Dec JE, Yang Y and Dronniou N. Boosted HCCI—controlling pressure-rise rates for performance improvements using partial fuel stratification with conventional gasoline. *SAE Int J Engine* 2011; 4: 1169–1189.
32. Tsurushima T, Kunishima E, Asaumi Y, Aoyagi Y and Enomoto Y. The effect of knock on heat loss in homogeneous charge compression ignition engines. SAE technical paper 2002-01-0108, 2002.
33. Splitter D. *High efficiency RCCI combustion*. Madison, WI: University of Wisconsin–Madison, 2012.
34. Gao S, Wang M and Lee C-F. NOx reduction in compression-ignition engine by inverted ignition phi-sensitivity. SAE technical paper 2017-01-0749, 2017.